IEICE Electronics Express, Vol.16, No.23, 1–4

LETTER

Dual-band substrate integrated waveguide dual-dumbbell-shaped-slot-fed patch antenna

Sheng Zhang[1], **YuYu Zhou**[1], **Ye Zhong**[1], **ShouFeng Tang**[1a)], **and Chao Ji**[1]

Abstract A dual-band low-profile substrate integrated waveguide (SIW) dual-dumbbell-shaped-slot-fed (DDSSF) patch antenna is presented in this letter. The antenna is designed using the dual-dumbbell-slot feeding structure in SIW and two patches to radiate. And it achieves two passbands by exciting two modes of dual dumbbell-shaped slots (DDSSs). The first impedance bandwidth is 4.1%, the second one is 10.0% and gains up to 6.7 dBi and 7.4 dBi, respectively. Furthermore, the two bands can be separated from each other and the cross-polarization level is below −30 dB. The simulation and measurement results of the proposed antenna are in good agreements.

Keywords: dual-wide-band, low cross-polarization, dumbbell-shaped slot, substrate integrated waveguide (SIW)

Classification: Microwave and millimeter-wave devices, circuits, and modules

1. Introduction

The growing of modern wireless communications have presented continue demands for wide bandwidth, small size and good radiation patterns antennas. Therefore, compared with microstrip antennas [1, 2, 3, 4, 5, 6, 7, 8, 9, 10, 11, 12, 13, 14, 15], due to the high quality factor, small radiation loss, light weight and easy integration, the design of antennas using substrate integrated waveguide (SIW) [16, 17, 18, 19, 20, 21, 22, 23, 24, 25] has been popular recently as a planar and integrated form of waveguide. But it also has shortcomings, especially the bandwidths may be narrow [22, 23] and the cross-polarization level is high [24, 25] because of the single feeding way. So, in these years, it is used to fed patch antenna as an approach of highly efficient driving method [26, 27, 28, 29, 30]. As a result, SIW series-fed or multi-layer SIWs are presented to excite the patch antenna. In [26], a LTCC SIW-fed-dipole array antenna is designed, but the cross-polarization level is low and it costs much. Then, several single band antennas fed by SIW are introduced in [27, 28, 29]. However, they have limited scope of applications and average cross-polarization level. A SIW-slot-fed thin beam-squint-free cavity antenna is designed in [30]. Though it has two passbands, the fractional bandwidth (FBW) is low.

In this paper, a novel dual-broad-band SIW patch antenna with dual-dumbbell-slot-fed is proposed and designed. By using the characteristic of two modes of the dual dumbbell-shaped slots (DDSSs) that is vertical to each other, it achieves not only two broad passbands that the first passband can be separated from the second band, but also improved cross-polarization performance in the whole impedance bandwidth. DDSSs is etched on the middle metal layer to excite the patches. For study the feature of the antenna, main parameter studies are put forward by simulations. Finally, a prototype is fabricated and measured. The measured results are in good agreements with the simulation ones.

2. The structure and design of the proposed antenna

2.1 DDSSF patch antenna

The 3-D view and top view of proposed SIW fed patch antenna are shown in Fig. 1 and the dimensions are shown in Table I. All parts of the antenna are fabricated using low-cost printed circuit board (PCB) process. It contains two dielectric substrate layers with the overall dimensions of $26 * 20\,\text{mm}^2$ $(0.57\lambda_0 * 0.44\lambda_0)$ and three metal layers where λ_0 refers to the free space wavelength at the lower frequency (6.65 GHz). The top layer is to radiate and corresponding to the dumbbell-shaped slots of the middle layer SIW feeding structure. The DDSSs is etched on the middle metal layer, which is fed by a probe. By changing the positions of the probe, the fundamental mode and other high order modes can be generated. Besides, in order to improve the performance of the first band, two matching vias are added.

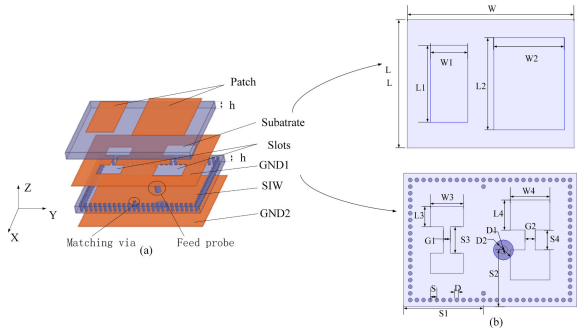

Fig. 1. The structure of the antenna. (a) 3-D view (b) top view ($W = 26\,\text{mm}$, $L = 20\,\text{mm}$, $W_1 = 5.8\,\text{mm}$, $L_1 = 12\,\text{mm}$, $W_2 = 11\,\text{mm}$, $L_2 = 14.4\,\text{mm}$, $W_3 = 5\,\text{mm}$, $L_3 = 3\,\text{mm}$, $W_4 = 4.5\,\text{mm}$, $L_4 = 6\,\text{mm}$, $G_1 = 1\,\text{mm}$, $G_2 = 1.5\,\text{mm}$, $S = 1\,\text{mm}$, $S_1 = 12\,\text{mm}$, $S_2 = 8.5\,\text{mm}$, $S_3 = 4\,\text{mm}$, $S_4 = 3\,\text{mm}$, $D = 0.6\,\text{mm}$, $D_1 = 1.2\,\text{mm}$, $D_2 = 3\,\text{mm}$)

[1]Dept. of Information and Control Engineering, China University of Ming and Technology, Xuzhou 22100, China
a) tsf0816@126.com

DOI: 10.1587/elex.16.20190624
Received October 8, 2019
Accepted October 28, 2019
Publicized November 15, 2019
Copyedited December 10, 2019

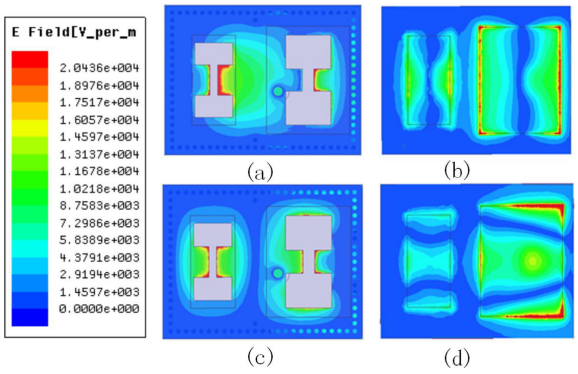

Fig. 2. Electric field density (a) on the middle metal layer at 6.65 GHz, (b) on the patches at 6.65 GHz, (c) on the middle metal layer at 11 GHz, (d) on the patches at 11 GHz

2.2 Parameter study

The electric field distributions at two frequencies are shown in Fig. 2. In Fig. 2(a)–(b), the lower frequency is ascribed to the resonance of the gap slots (denoted as gap mode). The electric field distributions are significantly distributed on left and right sides of the gap slots at 6.65 GHz and radiate from the long sides of the patches. The higher frequency is generated by the resonance of the lattice slots (denoted as lattice mode) in Fig. 2(c)–(d). The electric field distributed on up and down sides of the rectangular lattices at 11 GHz and radiate from the short sides. By using the gap mode and the lattice mode that is vertical to each other, it generates dual band and the bands are independent to each other as well.

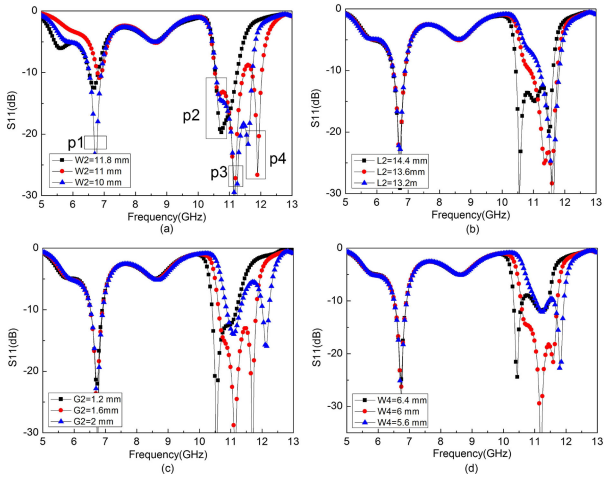

Fig. 3. Simulated S_{11} of different parameters (a) with various W_2, (b) with various L_2, (c) with various G_2, and (d) with various W_4.

To demonstrate the model analysis, studies on critical parameters are performed and discussed.

The first passband consists of one transmission pole (p_1), and the second passband contains three transmission poles, p_2, p_3 and p_4, respectively. Here, in Fig. 3(a), an increase in parameter W_2 from 10 mm to 11.8 mm will make the p_3 and p_4 shift to lower frequencies, while the p_1 and p_2 stays unchanged. It is found in Fig. 3(b) that the p_2 showed the most noticeable decreasing while p_3 and p_4 are almost unchanged as the L_2 changes from 12.2 mm to 14.4 mm. The variation of W_4 and G_2 can also be observed in Fig. 3(c) and (d). As G_2 shifts from 1.2 mm to 2 mm, the second band increases, in the meantime, p_1 remains the same. Likewise, the W_4 can also make the second band move to higher frequencies.

In conclusion, Fig. 3 shows the effects of the sizes of the slots and patches at two bands. The higher band shifts when the parameters change while the lower band is not affected. The parameter studies agree with the mode analysis.

3. Simulation and measurement results

The prototype antenna was fabricated and measured in Fig. 4. RT/duroid5880 with $\varepsilon_r = 2.2$, $\tan\delta = 0.0009$ and thickness $h = 1.575$ mm is used for the design. It is shown that the measured results are in excellent agreement with the simulated ones. The measured and the simulated impedance bandwidths are 4.1% (6.74 GHz–6.83 GHz) and 10.0% (10.44 GHz–11.65 GHz) respectively. The simulated and measured peak gains in two operation bands and the test scenarios are shown in Fig. 5. And the simulated and measured peak gains are 6.7 dBi at 6.65 GHz and 7.4 dBi at 11 GHz respectively.

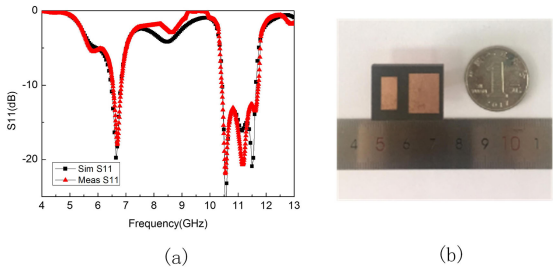

Fig. 4. (a) Simulated and measured S_{11} and gain of the proposed antenna, (b) photograph of the fabricated the proposed antenna.

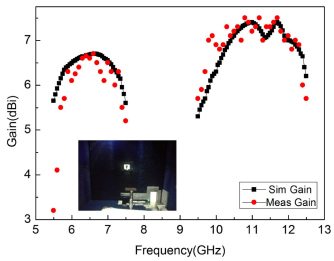

Fig. 5. The simulated and measured gains and test scenarios.

Radiation performances of the proposed antenna have been measured as shown in Fig. 6. It can be seen that the antenna resulted in wide beam and highly symmetric radiation profile in both the E and H planes. There is a good agreement between simulated and measured results. Furthermore, the measured cross-polarization level is below −30 dB and −35 dB in E-plane and H-plane in the operating band, respectively. Table I lists the main performance comparison of our work and other published antenna elements. From the table, the proposed antenna has a better performance by providing wide impedance bandwidth, high cross-polarization level compared with other antennas.

Table I. Comparison with previously reported antennas

Reference	Central frequency (GHz)	Size ($\lambda_0 * \lambda_0$)	Type	Layers	−10 dB FBW (%)	X-pol (dB)
Ref [24]	60	-na	aperture-coupled patch antenna	single-layer	1.8%	−20
Ref [25]	7.65	$0.7 * 0.6$	cavity-backed slot antenna	single-layer	3.26%	−15
Ref [26]	28	$0.82 * 0.6$	SIW-fed dipole antenna	double-layer	8.5%	−25
Ref [28]	10	-na	SIW-fed loop antenna	double-layer	4.1%	21
Ref [29]	31	$0.93 * 0.93$	SIW-fed planar antenna	double-layer	5.2%	−22
This work	11	$0.57 * 0.44$	SIW-fed patch antenna	double-layer	10.0%	−30

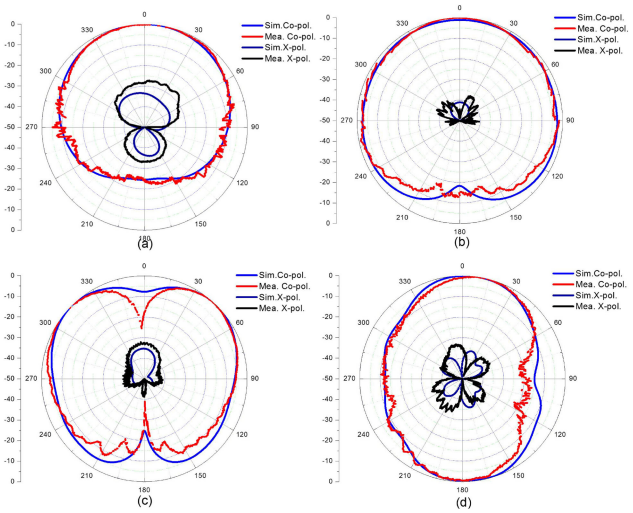

Fig. 6. Simulated and measured radiation patterns of the proposed antenna (a) at 6.65 GHz in E-plane, (b) at 6.65 GHz in H-plane, (c) at 11 GHz in E-plane, (d) at 11 GHz in H-plane.

4. Conclusion

In this paper, a novel dual-wide-band SIW DDSSF patch antenna is designed, fabricated and measured. The dual broad band is achieved by two SIW modes, and the two bands are independent of each other. The bandwidth of the second band can be changed by changing the sizes of the slots and patches while the first band stays unchanged. And the two orthogonal modes of DDSSs improve the cross-polarization level at the whole impedance bandwidth. Besides, the proposed antenna still keeps many advantages such as light weight, low fabrication cost and easy to integrate with planar circuits.

Acknowledgments

This work is supported by National Key R&D Program of China 2017YFF0205500.

References

[1] D. Feng, *et al.*: "A broadband low-profile circular-polarized antenna on an AMC reflector," IEEE Antennas Wireless Propag. Lett. **16** (2017) 2840 (DOI: 10.1109/LAWP.2017.2749246).

[2] F. Sun, *et al.*: "A frequency diversity printed-Yagi antenna element for apertures selectivity wideband array application," IEEE Trans. Antennas Propag. **66** (2018) 5634 (DOI: 10.1109/TAP.2018.2855722).

[3] M. Shirazi, *et al.*: "A switchable-frequency slot-ring antenna element for designing a reconfigurable array," IEEE Antennas Wireless Propag. Lett. **17** (2017) 229 (DOI: 10.1109/LAWP.2017.2781463).

[4] M. Shirazi, *et al.*: "A reconfigurable dual-polarization slot-ring antenna element with wide bandwidth for array applications," IEEE Trans. Antennas Propag. **66** (2018) 5943 (DOI: 10.1109/TAP.2018.2863110).

[5] Y. Yang, *et al.*: "A low-cost, single-layer, dual circularly polarized antenna for millimeter-wave applications," IEEE Antennas Wireless Propag. Lett. **18** (2019) 651 (DOI: 10.1109/LAWP.2019.2900301).

[6] Z. Tang, *et al.*: "Wideband differentially fed dual-polarized planar antenna and its array with high common-mode suppression," IEEE Trans. Antennas Propag. **67** (2019) 131 (DOI: 10.1109/TAP.2018.2878284).

[7] J. Ren, *et al.*: "Low-RCS monopolar patch antenna based on a dual-ring metamaterial absorber," IEEE Antennas Wireless Propag. Lett. **17** (2017) 102 (DOI: 10.1109/LAWP.2017.2776978).

[8] R. Lian, *et al.*: "Design of a broadband polarization-reconfigurable Fabry-Perot resonator antenna," IEEE Antennas Wireless Propag. Lett. **17** (2018) 122 (DOI: 10.1109/LAWP.2017.2777502).

[9] J. Liu, *et al.*: "Gain enhancement of a broadband symmetrical dual-loop antenna using shorting pins," IEEE Antennas Wireless Propag. Lett. **17** (2018) 1369 (DOI: 10.1109/LAWP.2018.2844293).

[10] H. Li, *et al.*: "A low-profile dual-polarized microstrip antenna array for dual-mode OAM applications," IEEE Antennas Wireless Propag. Lett. **16** (2017) 3022 (DOI: 10.1109/LAWP.2017.2758520).

[11] Y. Liu, *et al.*: "A dual-polarized dual-band antenna with omni-directional radiation patterns," IEEE Trans. Antennas Propag. **65** (2017) 4259 (DOI: 10.1109/TAP.2017.2708093).

[12] X. Yang, *et al.*: "Analysis and design of a broadband multifeed tightly coupled patch array antenna," IEEE Antennas Wireless Propag. Lett. **17** (2018) 217 (DOI: 10.1109/LAWP.2017.2780992).

[13] X. Yi, *et al.*: "A double-layer wideband transmitarray antenna using two degrees of freedom elements around 20 GHz," IEEE Trans. Antennas Propag. **67** (2019) 2798 (DOI: 10.1109/TAP.2019.2893265).

[14] H. Huang, *et al.*: "A broadband dual-polarized base station antenna with sturdy construction," IEEE Antennas Wireless Propag. Lett. **16** (2017) 665 (DOI: 10.1109/LAWP.2016.2598181).

[15] L. Wen, *et al.*: "Compact dual-polarized shared-dipole antennas for base station applications," IEEE Trans. Antennas Propag. **66** (2018) 6826 (DOI: 10.1109/TAP.2018.2871717).

[16] T. Cheng, *et al.*: "Broadband SIW cavity-backed modified dumbbell-shaped slot antenna," IEEE Antennas Wireless Propag. Lett. **18** (2019) 936 (DOI: 10.1109/LAWP.2019.2906119).

[17] S. Park and S. Park: "LHCP and RHCP substrate integrated waveguide antenna arrays for millimeter-wave applications," IEEE Antennas Wireless Propag. Lett. **16** (2017) 601 (DOI: 10.1109/LAWP.2016.2594081).

[18] L. Sun, *et al.*: "Low-profile, quasi-omnidirectional substrate integrated waveguide (SIW) multihorn antenna," IEEE Antennas Wireless Propag. Lett. **15** (2016) 818 (DOI: 10.1109/LAWP.2015.2476346).

[19] L. Tan, *et al.*: "Magnetically reconfigurable SIW antenna with tunable frequencies and polarizations," IEEE Trans. Antennas Propag. **63** (2015) 2772 (DOI: 10.1109/TAP.2015.2414446).
[20] C. Fan, *et al.*: "A low cross-polarization reflectarray antenna based on SIW slot antenna," IEEE Antennas Wireless Propag. Lett. **16** (2017) 333 (DOI: 10.1109/LAWP.2016.2574888).
[21] F. Ren, *et al.*: "Three-dimensional SIW-driven microstrip antenna for wideband linear and circular polarization applications," IEEE Antennas Wireless Propag. Lett. **16** (2017) 2400 (DOI: 10.1109/LAWP.2017.2720627).
[22] H. Jamshidi-Zarmehri and M. H. Neshati: "Design and development of high-gain SIW H-plane horn antenna loaded with waveguide, dipole array, and reflector nails using thin substrate," IEEE Trans. Antennas Propag. **67** (2019) 2813 (DOI: 10.1109/TAP.2019.2896445).
[23] Z. Zhang, *et al.*: "Broadband SIW cavity-backed slot antenna for endfire applications," IEEE Antennas Wireless Propag. Lett. **17** (2018) 1271 (DOI: 10.1109/LAWP.2018.2842046).
[24] T. Mikulasek, *et al.*: "Design of aperture-coupled microstrip patch antenna array fed by SIW for 60 GHz band," IET Microw. Antennas Propag. **10** (2016) 288 (DOI: 10.1049/iet-map.2015.0296).
[25] A. Kumar and S. Raghavan: "A self-triplexing SIW cavity-backed slot antenna," IEEE Antennas Wireless Propag. Lett. **17** (2018) 772 (DOI: 10.1109/LAWP.2018.2815665).
[26] M. Du, *et al.*: "LTCC SIW-vertical-fed-dipole array fed by a microstrip network with tapered microstrip-to-SIW transitions for wideband millimeter-wave applications," IEEE Antennas Wireless Propag. Lett. **16** (2017) 1953 (DOI: 10.1109/LAWP.2017.2690325).
[27] M. E. Lajevardi and M. Kamyab: "Ultraminiaturized metamaterial-inspired SIW textile antenna for off-body applications," IEEE Antennas Wireless Propag. Lett. **16** (2017) 3155 (DOI: 10.1109/LAWP.2017.2766201).
[28] L. Lu, *et al.*: "Design of low-sidelobe circularly polarized loop linear array fed by the slotted SIW," IEEE Antennas Wireless Propag. Lett. **16** (2017) 537 (DOI: 10.1109/LAWP.2016.2587780).
[29] F. Ren, *et al.*: "Polarization-adjustable planar array antenna with SIW-fed high-order-mode microstrip patch," IEEE Trans. Antennas Propag. **65** (2017) 6167 (DOI: 10.1109/TAP.2017.2756686).
[30] W. Liu, *et al.*: "SIW-slot-fed thin beam-squint-free Fabry-Perot cavity antenna with low backlobe levels," IEEE Antennas Wireless Propag. Lett. **13** (2014) 552 (DOI: 10.1109/LAWP.2014.2311813).